VOL. 22, NO. 2, 2023, 8-13
elektrika.utm.my
ISSN 0128-4428

ELEKTRIKA
Journal of Electrical Engineering

3D Image Reconstruction Capability of Peripheral On-chip ECT Sensor

Gooi Wen Pin[1], **Leow Pei Ling**[1*], **Jaysuman Pusppanathan**[1,2], **Hor Xian Feng**[1] and **Shahrulnizahani Mohammad Din**[1]

[1]Faculty of Electrical Engineering, Universiti Teknologi Malaysia, 81310 UTM Skudai, Johor, Malaysia.
[2]Sport Innovation & Technology Centre (SiTC), Institute of Human Centered Engineering (iHumen), Universiti Teknologi Malaysia, Block V01, 81310 Skudai Johor, Malaysia.
[*]Corresponding author: leowpl@utm.my

Abstract: The miniaturisation of electrical tomography sensors such as EIT has become popular recently and these miniaturised sensors were investigated for 2D and 3D imaging of cells in EIT. Nevertheless, research on miniaturisation of ECT sensor also existed which were based on peripheral electrode sensor which had electrodes arranged on the surface around the sensing chamber. However, the study on the miniature peripheral ECT sensor was limited to 2D image reconstruction and detection of presents of samples in the sensing chamber only and lacked the works on the 3D imaging capability. Therefore, this article investigates the 3D image reconstruction capability of peripheral on-chip ECT sensor through simulation approach by simulating a cube phantom at several test positions in the sensing chamber. Eventually, the 3D and 2D images were reconstructed and the 3D imaging capability of the sensor was characterised qualitatively based on visual inspection of the reconstructed image. The simulation results revealed that the 3D imaging capability of peripheral on-chip ECT sensor was limited to the region where electrodes were present only. However, the 2D reconstructed image results showed that the sensor was able to locate the positions of test phantom in the sensing chamber accurately.

Keywords: 2D ECT, 3D ECT, lab-on-chip, peripheral electrode sensor

Article History: received 28 February 2023; accepted 26 July 2023; published 28 August 2023.

1. INTRODUCTION

The 2D electrical capacitance tomography (ECT) is well-established for cross-sectional visualisation of permittivity distribution in application such as detecting the position of surface defect [1], monitoring of fluidised bed processes [2] [3] and monitoring of flow regime in pipeline [4]. The 2D ECT was rather simpler as the number of pixels involved often lesser than the number of pixels required for 3D ECT. With the introduction of method of generating the sensitivity distribution based on the electric field distribution, it simplifies the work and time required to generate the sensitivity maps of 3D ECT sensors [5]. The 3D ECT has become an important tools in industrial process imaging because the conventional 2D ECT failed to provide accurate and complete information on a process [6]. As compared to 2D ECT, the 3D ECT provides additional information such as the volumetric data related to the process under investigation [7], [8], [9]. The 3D ECT has been explored for applications such as image fusion for flame imaging [10] and imaging of two-phase flow [11] which utilised ECT sensor that has more than one electrode plane. Besides, 3D image reconstruction based on planar ECT was particularly useful in subsurface object detection because 3D ECT involves an additional vertical dimension which penetrates into the surface [12].

In recent decade, the miniaturisation of electrical tomography sensor array has been blooming with the advancement of microfluidics and lab-on-chip applications. The electrical impedance tomography (EIT) sensor array for example, has been miniaturised to fit in miniature sensing chamber of sizes ranging from 12 mm to 35 mm and the size of microelectrodes ranges from 0.6 mm to 5 mm [13], [14], [15], [16]. The miniature EIT sensors has been investigated in 3D imaging of cells [17], 2D visualisation of drug responds on cells in scaffolds [18] and 3D imaging of 3D cultured cells in scaffold [13].

The feasibility of miniature ECT sensor was investigated by [19] for lab-on-chip applications and showed that the capacitance measurement could be measured and agreed with the simulated capacitance trend. Meanwhile, [20] investigated the 2D imaging of multiphase flow using miniature ECT sensor and the reconstructed 2D images showed high similarity to the camera-captured image. Besides, [21] performed a simulation study using miniature ECT sensor on the sensing of yeast cells and the results showed that miniature ECT sensor could detect the presence of yeast cell model. Furthermore, [22] attempted the 3D image reconstruction of two-phase fluid and found that the miniature ECT sensor could provide information on the height and the location of test sample based on the different vertical layer of 2D image.

The miniature ECT sensor design of the existing works was based on planar peripheral electrode design whereby

the electrodes were arranged on the surface around the circumference of the sensing chamber. The current performance of the miniature ECT sensors were investigated for 2D image reconstruction only and the reconstructed 2D image can describe the position of the sample correctly but does not provide information regarding the height of sample. Through 3D image reconstruction, both the position and height of the sample could be visualised by considering the z-axis performance of the miniature ECT sensor. The additional height information provided by 3D image reconstruction could be beneficial in application that require volumetric estimation of the sample. However, there are limited studies on 3D image reconstruction capability of the miniature ECT sensor based on peripheral electrode design. Therefore, this article investigates on the 3D image reconstruction capability of the peripheral on-chip ECT sensor by considering the performance in z-axis. The investigation was performed through numerical simulation. A 2 mm cube phantom was placed at several positions in the sensing chamber and the 2D and 3D image were reconstructed using linear back projection algorithm (LBP). The 3D image reconstruction capability of the sensor was characterised quantitatively using correlation coefficient (CC) and the percentage height error.

2. NUMERICAL SIMULATION

2.1 Sensor model

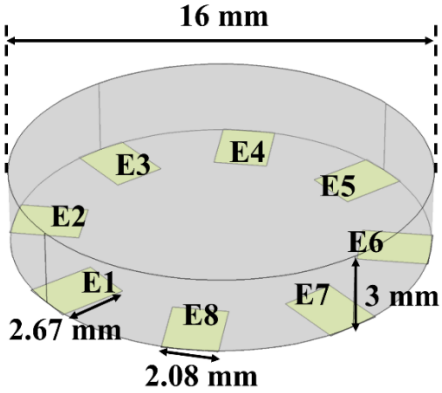

Figure 1. Sensor model of peripheral on-chip ECT sensor

To investigate the 3D imaging capability of the peripheral on-chip ECT sensor, the optimised sensor design from [20] has been adopted with parameters as illustrated in Figure 1. The sensor was modelled in 3D instead of 2D to obtain the distribution of electric field in the z-axis direction which is vital for height sensing. The peripheral on-chip ECT sensor consisted of eight electrodes which were arranged around the circumference of the sensing chamber. The electrodes were rectangle in shape with a length of 2.67 mm and width of 2.08 mm. According to [20], the electrodes were peripherally arranged to obtain capacitance measurement from different angles through the fan beam projection which enhance the resolution of reconstructed image. Meanwhile, the length of the electrode was chosen as 2.67 mm so that the electric field reaches the top of sensing chamber for thorough sensitivity coverage. Further increasing the length of electrodes will result in lower penetration of electric field in the z-axis direction as the gap between opposite electrode (E1-E5) is narrow, thus lowering the height sensing of sensor. The electrodes were radially arranged around the sensing chamber whereby the angle between two neighbouring electrodes was 45°. The electrodes were designed to fit into a sensing chamber with a height of 3 mm and a diameter of 16 mm. The sensor model of peripheral on-chip ECT sensor was simulated in 3D using COMSOL Multiphysics. The electric field between all possible electrode pairs were simulated and used in the computation of 3D sensitivity map for 3D image reconstruction. In this study, the sensing chamber was discretised into 10240 voxels in total and it composed of 32 × 32 voxels in the x-y plane and 10 layers along the z-axis. The 2D sensitivity map was obtained by extracting the first layer of the 3D sensitivity map.

2.2 Simulation image reconstruction

The simulation image reconstruction was performed by placing a test phantom at several test positions in the sensing chamber as shown in Figure 2.

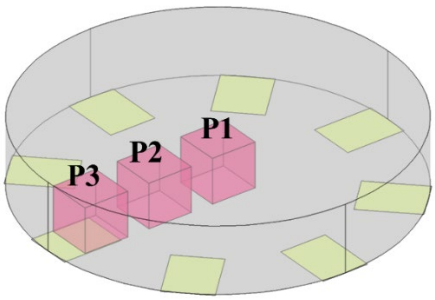

Figure 2. Test position of cube phantom in peripheral on-chip ECT sensor

As illustrated in Figure 2, a 2 mm cube phantom was used in the 2D and 3D image reconstruction simulation. The permittivity of the cube phantom was set to 190 while the background permittivity was set to 1 so that permittivity contrast was present between the cube phantom and the background. The cube phantom was placed at test positions P1, P2 and P3 one at a time. Then, the interelectrode capacitance measurement was simulated in COMSOL Multiphysics. Eventually, the simulated interelectrode capacitance measurements were exported and the 2D and 3D image were reconstructed using LBP in MATLAB.

3. RESULTS AND DISCUSSION

Figure 3 shows the reconstructed 2D image of the 2 mm cube phantom at test positions P1, P2 and P3. A red dotted boundary is superimposed onto the 2D image to represent the actual position of the cube phantom at each test position. Meanwhile, Figure 4 illustrates the 3D reconstructed image of the cube phantom in 2D slices along the z-axis. The colour bars in Figure 3 and Figure 4 show the permittivity distribution in the sensing chamber with yellow representing high permittivity and blue representing low permittivity. The numbers on the colour bar ranging from 0 to 1.0 represent the lowest to the highest scale of the permittivity distribution. In this study, the

yellow region indicates the reconstructed cube phantom while the blue region indicates the background medium. Figure 5 present the synthesised 3D isosurface image based on the 2D slices. The actual cube phantom is superimposed on the 3D isosurface image for references.

As shown in Figure 3, the peripheral on-chip ECT sensor successfully reconstructs 2D image at all the test positions. The reconstructed 2D image of the cube phantom falls within the actual position of the cube phantom. The 2D imaging results indicated that the peripheral on-chip ECT sensor can locate the presence of samples in the sensing chamber. However, the 2D image quality was limited to displaying the cube phantom in the form of circular shades only and the height cannot be visualised.

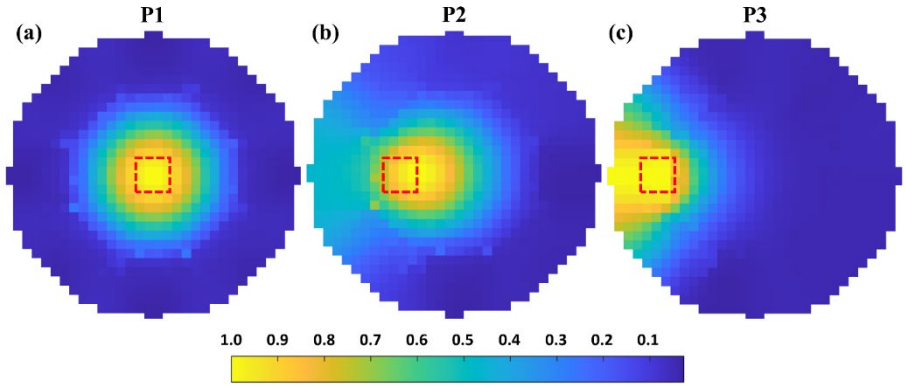

Figure 3. 2D reconstructed image of cube phantom at test positions P1, P2 and P3

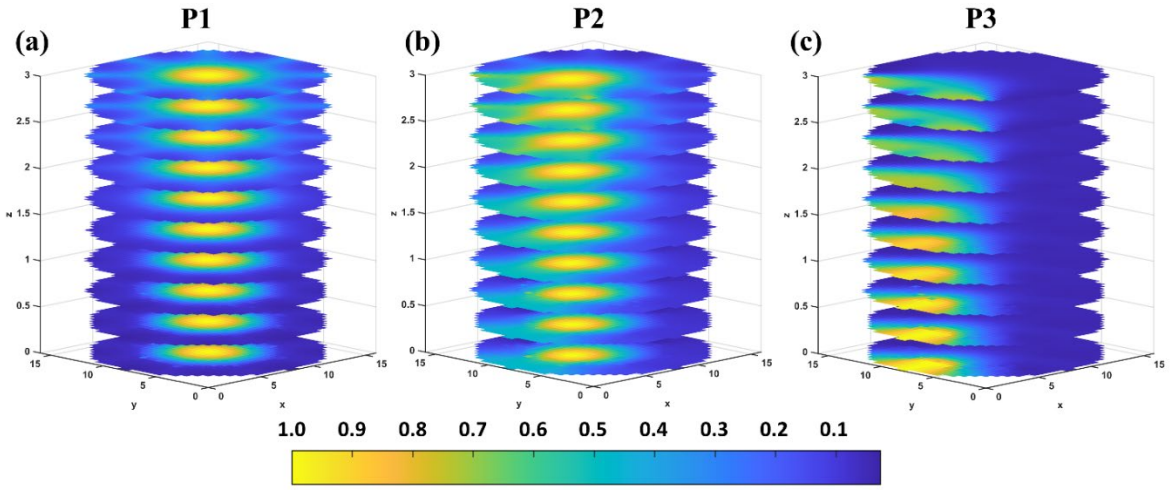

Figure 4. 3D reconstructed image of cube phantom at test positions P1, P2 and P3 presented in 2D slices

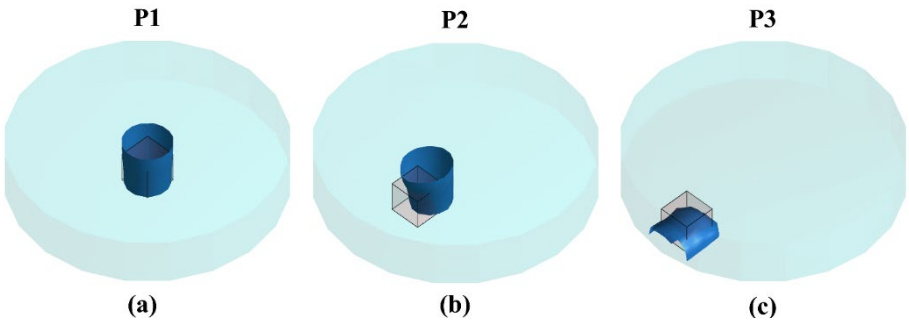

Figure 5. Synthesised isosurface representation of 3D reconstructed image of cube phantom at test positions P1, P2 and P3

The primary interest of 3D image reconstruction is the reconstruction of the height of sample in the sensing chamber. As illustrated in Figure 4 and Figure 5, the 3D imaging performance of peripheral on-chip ECT sensor is dependent on the position of cube phantom in the sensing chamber. The reconstructed 3D image revealed that the height of cube phantom was able to be reconstructed when the cube phantom was positioned above the electrode at test position P3. Although the height of cube phantom was reconstructed lower than the actual height of cube phantom, the peripheral on-chip ECT sensor showed the ability to resolve the height of test sample.

Meanwhile, the reconstructed 3D images at test positions P1 and P2 showed that the height of cube phantom failed to be resolve as the reconstructed height extended from bottom to the top of sensing chamber. The test positions P1 and P2 were both located away from the electrodes. Based on the 3D image reconstruction results, it was deduced that the 3D imaging capability of peripheral on-chip ECT sensor is limited to the location where electrodes are present only.

The quality of the reconstructed 3D image was quantitatively evaluated using CC which is given by

$$CC = \frac{\sum_{i=1}^{N}(\varepsilon_i - \bar{\varepsilon})(\hat{\varepsilon}_i - \bar{\hat{\varepsilon}})}{\sqrt{\sum_{i=1}^{N}(\varepsilon_i - \bar{\varepsilon})^2 \sum_{i=1}^{N}(\hat{\varepsilon}_i - \bar{\hat{\varepsilon}})^2}}$$

where N is the number of voxels which in this study is 10240 while ε and $\hat{\varepsilon}$ are the reconstructed image and cube phantom, respectively. $\bar{\varepsilon}$ and $\bar{\hat{\varepsilon}}$ are the means of ε and $\hat{\varepsilon}$, respectively. The CC evaluate the resemblance of the reconstructed 3D image to the actual cube phantom. Meanwhile, the height of reconstructed 3D image was evaluated using the percentage height error given by

$$E_h = \frac{h_{reconstructed} - h_{actual}}{h_{actual}} \times 100\%$$

where E_h is the percentage height error, $h_{reconstructed}$ is the height of reconstructed 3D image and h_{actual} is the height of the cube phantom. Figure 6 shows the CC and the percentage height error of the reconstructed 3D images at test positions P1, P2 and P3.

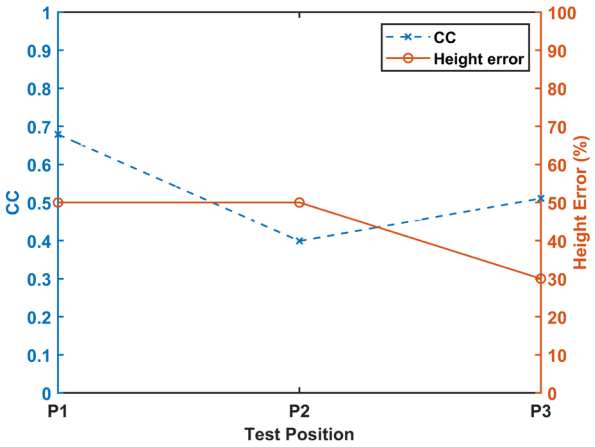

Figure 6. The CC and height error of reconstructed 3D image of cube phantom

Figure 6 shows that the extended reconstructed height from bottom to the top of sensing chamber at test positions P1 and P2 resulted in 50% height error. Meanwhile, a lower height error of 30% is reconstructed at test position P3 where the electrodes are located. The decrease in height error and the increase in CC of the reconstructed 3D image from test position P2 to P3 suggest that the quality of reconstructed 3D image is improved when the object is placed near to the electrodes. However, the CC of reconstructed 3D image at test position P1 is the highest despite having 50% height error. A high CC is computed at test position P1 because the reconstructed 3D image fully occupies the reference cube as illustrated in Figure 5 (a) indicating low difference between the reconstructed 3D image and the cube phantom along the horizontal x and y axis.

To investigate the underlaying reason of the limited 3D imaging capability of peripheral on-chip ECT sensor, the axial resolution analysis was performed on the sensitivity map of peripheral on-chip ECT sensor. The axial resolution analysis analysed the sensitivity distribution of peripheral on-chip ECT sensor along the z-axis which correspond to the height reconstruction at different location of x-y plane. Figure 7 shows the axial resolution analysis plot of peripheral on-chip ECT sensor.

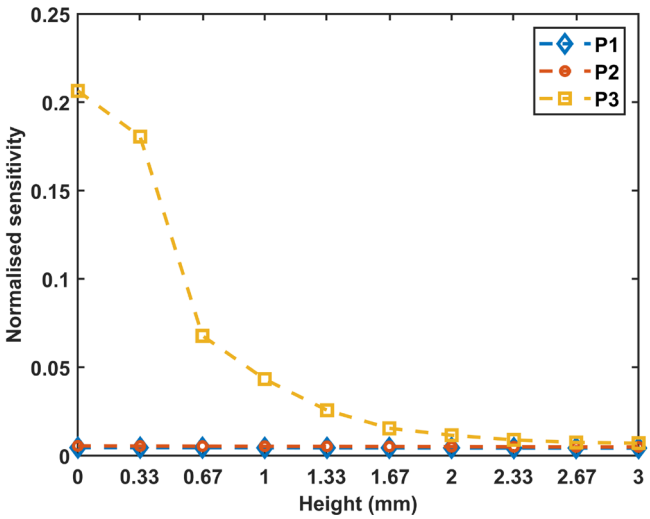

Figure 7. Axial resolution analysis at test positions P1, P2 and P3

Based on Figure 7, it can be deduced that the sensitivity variation along z-axis is needed for peripheral on-chip ECT sensor to reconstruct the height of cube phantom in 3D image reconstruction. When the cube phantom was placed at test position P3 which has variation in sensitivity along z-axis, the height of the 3D image of cube phantom can be resolved. Besides, the reconstructed height of cube phantom was lower than the actual height of 2 mm and this corresponds to the lower magnitude of sensitivity distribution when the height from electrode surface approaches 2 mm.

Meanwhile at test positions P1 and P2, the reconstructed height of cube phantom extended from bottom the top of sensing chamber because these test positions lacked variation in sensitivity along z-axis. As illustrated in

Figure 7, the sensitivity distribution magnitude at test positions P1 and P2 remained constant along the z-axis. Therefore, the reconstructed 3D images have equal contrast from bottom to the top of sensing chamber.

4. CONCLUSION

In this article, the 2D and 3D imaging capability of peripheral on-chip ECT sensor was investigated through simulation approach. The simulation results revealed that the peripheral on-chip ECT sensor was able to reconstruct 2D images of cube phantom at all the test positions correctly. The 3D image reconstruction results, however, showed that the height of the reconstructed 3D image of cube phantom was not necessarily correct although the position of the cube phantom was correctly reconstructed in 2D image reconstruction. It was found that the variation of sensitivity distribution along the z-axis was necessary for peripheral on-chip ECT sensor to reconstruct the height of cube phantom in 3D image reconstruction. The sensitivity variation along z-axis was identified to be found in region where the electrodes were located only. Based on the findings in this article, the peripheral on-chip ECT sensor was not practical for ECT applications that require 3D image reconstruction because the height of the reconstructed image varies with position. The design of planar electrode arrays for 3D ECT should be made such that sensitivity variation is present throughout the sensing chamber so that the height of 3D reconstructed image can be resolved at all locations within the sensing chamber.

ACKNOWLEDGMENT

This work was supported by the Ministry of Higher Education Malaysia and Universiti Teknologi Malaysia for all financial support through FRGS Project code: FRGS/1/2020/TK0/UTM/02/47.

REFERENCES

[1] S. Amato, D. A. Hutchins, X. Yin, M. Ricci, and S. Laureti, “Capacitive imaging using fused amplitude and phase information for improved defect detection,” *NDT E Int.*, vol. 124, no. August, p. 102547, 2021.

[2] H. Wang and W. Yang, “Application of electrical capacitance tomography in pharmaceutical fluidised beds – A review,” *Chem. Eng. Sci.*, vol. 231, no. xxxx, p. 116236, Feb. 2021.

[3] K. Huang *et al.*, “Effect of Electrode Length of an Electrical Capacitance Tomography Sensor on Gas−Solid Fluidized Bed Measurements,” *Ind. Eng. Chem. Res.*, vol. 58, no. 47, pp. 21827–21841, Nov. 2019.

[4] L. Zhang and W. Yin, “Image reconstruction method along electrical field centre lines using a modified mixed normalization model for electrical capacitance tomography,” *Flow Meas. Instrum.*, vol. 62, no. May, pp. 37–43, 2018.

[5] A. Fabijańska and R. Banasiak, “Graph convolutional networks for enhanced resolution 3D Electrical Capacitance Tomography image reconstruction,” *Appl. Soft Comput.*, vol. 110, p. 107608, 2021.

[6] R. Wajman and R. Banasiak, “Tunnel-based method of sensitivity matrix calculation for 3D-ECT imaging,” *Sens. Rev.*, vol. 34, no. 3, pp. 273–283, Jun. 2014.

[7] M. R. Baidillah, M. Mukhlisin, and W. P. Taruno, “Comparisons of sensor geometries for electrical capacitance volume tomography,” *Int. J. Innov. Comput. Inf. Control*, vol. 9, no. 11, pp. 4447–4457, 2013.

[8] Q. Marashdeh, L.-S. Fan, B. Du, and W. Warsito, “Electrical Capacitance Tomography − A Perspective,” *Ind. Eng. Chem. Res.*, vol. 47, no. 10, pp. 3708–3719, May 2008.

[9] I. K. Ahmad, M. Mukhlisin, and H. Basri, “Comparisons of Sensor Position for Electrical Capacitance Volume Tomography (Ecvt),” *Mod. Appl. Sci.*, vol. 10, no. 4, p. 150, Feb. 2016.

[10] S. Sun *et al.*, “Sensitivity Guided Image Fusion for Electrical Capacitance Tomography,” *IEEE Trans. Instrum. Meas.*, vol. 70, no. c, pp. 1–12, 2021.

[11] S. Sun, X. Lu, L. Xu, Z. Cao, J. Sun, and W. Yang, “Real-Time 3-D Imaging and Velocity Measurement of Two-Phase Flow Using a Twin-Plane ECT Sensor,” *IEEE Trans. Instrum. Meas.*, vol. 70, 2021.

[12] P. Suo, J. Sun, W. Tian, S. Sun, and L. Xu, “3-D Image Reconstruction in Planar Array ECT by Combining Depth Estimation and Sparse Representation,” *IEEE Trans. Instrum. Meas.*, vol. 70, 2021.

[13] Y. Yang, H. Wu, J. Jia, and P. O. Bagnaninchi, “Scaffold-Based 3-D Cell Culture Imaging Using a Miniature Electrical Impedance Tomography Sensor,” *IEEE Sens. J.*, vol. 19, no. 20, pp. 9071–9080, 2019.

[14] H. Wu, W. Zhou, Y. Yang, J. Jia, and P. Bagnaninchi, “Exploring the potential of electrical impedance tomography for tissue engineering applications,” *Materials (Basel).*, vol. 11, no. 6, pp. 1–11, 2018.

[15] M. Lemmens, H. Biesmans, S. Bormans, T. Vandenryt, and R. Thoelen, “Electrical Impedance Tomography With a Lab-on-Chip for Imaging Cells in Culture,” *Phys. status solidi*, vol. 215, no. 15, p. 1700868, Aug. 2018.

[16] G. Ma and M. Soleimani, “A new label-free and contactless bio-tomographic imaging with miniaturized capacitively-coupled spectroscopy measurements,” *Sensors (Switzerland)*, vol. 20, no. 11, pp. 1–19, 2020.

[17] Y. Yang, J. Jia, S. Smith, N. Jamil, W. Gamal, and P. O. Bagnaninchi, “A miniature electrical impedance tomography sensor and 3-D Image Reconstruction for Cell Imaging,” *IEEE Sens. J.*, vol. 17, no. 2, pp. 514–523, 2017.

[18] H. Wu, Y. Yang, P. O. Bagnaninchi, and J. Jia, “Imaging cell-drug response in 3D bioscaffolds by electrical impedance tomography,” in *2017 IEEE International Conference on Imaging Systems and Techniques (IST)*, 2017, vol. 2018-Janua, no. 2, pp. 1–5.

[19] A. Azmi, R. A. Rahim, P. S. Chee, S. M. Din, N. M. N. Ayob, and P. L. Leow, “Miniaturized planar sensor development,” *J. Teknol. (Sciences Eng.*, vol. 69, no. 8, pp. 101–105, 2014.

[20] N. A. Mohd Razali, "On Chip Planar Capacitance Tomography for Two-Phase Fluid Flow Imaging," 2016.

[21] N. A. Zulkiflli *et al.*, "Finite Element Analysis for Yeast Cells using Electrical Capacitance Tomography," in *Proceedings of the 2019 IEEE International Conference on Signal and Image Processing Applications, ICSIPA 2019*, 2019, pp. 346–350.

[22] H. X. Feng *et al.*, "Simulation Study of Two-Phase Fluid 3D Imaging Using Lab-on-Chip ECT," in *2019 IEEE International Conference on Signal and Image Processing Applications (ICSIPA)*, 2019, pp. 259–263.